EDAP+ TN on Methods and Reference Data for Optical Data quality Assessments

Author(s):

Digitally signed by Dr Samantha Lavender
DN: cn=Dr Samantha Lavender, o, ou,
email=sam.lavender@telespazio.com, c=US
Date: 2023.07.12 16:22:01 +01'00'

Fay Done
Pauline Cocevar
Samantha Lavender
Sébastien Saunier
Task 2 Team

Approval:

Amy Beaton
EDAP+ Service Manager

Accepted:

Clément Albinet
EDAP+ Technical Officer

AMENDMENT RECORD SHEET

The Amendment Record Sheet below records the history and issue status of this document.

ISSUE	DATE	REASON
0.1	01 March 2023	First draft issue for ESA review
0.2	14 June 2023	Deleted summary based on ESA feedback, plus updated to included MTF assessment in Appendix A
1.0	12 July 2023	Revised Section 2.2.1.1.2 based on ESA feedback

TABLE OF CONTENTS

1. EXECUTIVE SUMMARY

The **Earthnet Data Assessment Project** (**EDAP+**) optical team produces preliminary assessments of data (e.g. geometric calibration, radiometric calibration and image quality) from New Space **Very High Resolution (VHR) to High Resolution (HR) Optical Earth Observation** (**EO**) **missions** that have been selected for potential inclusion in the European Space Agency (**ESA**) Earthnet Programme as a Third Party Mission (**TPM**). The optical team uses a variety of methodologies, based on best practices and guidelines (e.g. Quality Assurance Framework for Earth Observation (**QA4EO**) [RD-1], EDAP Quality Assessment Framework [RD-2, RD-3]), tools and reference data for their assessments and these are documented here.

The MTF_Estimator QGIS plug-in was assessed as being suitable for use in modulation transfer function (**MTF**) assessment; it can be noted that no other freely available suitable software was accessible at the time of the writing of this report, but this may subject to change.

Note this document will continue to be updated, to ensure that all information relating to the adopted methodologies, tools and reference data used in the assessments, typically of standard Level 1 products (geometrically and radiometrically calibrated), is current.

1.1 References

The following is a list of reference documents with a direct bearing on the content of this report. Where referenced in the text, these are identified as [RD-n], where 'n' is the number in the list below:

RD-1. QA4EO, https://qa4eo.org/ Accessed online: 23 February 2023

RD-2. EDAP Best Practice Guidelines, EDAP.REP.001, v2.2, 6 December 2022

RD-3. Earth Observation Mission Quality Assessment Framework – Optical Guidelines, EDAP.REP.002, v2.1, 31 October 2021

RD-4. QGIS, https://www.qgis.org/en/site/ Accessed online: 23 February 2023

RD-5. SPOT Image Quality Performances, CNES C443-NT-0-296-CN, https://www.intelligence-airbusds.com/files/pmedia/public/r438_9_spot_quality_performances_2013.pdf Accessed online: 23 February 2023

RD-6. EDAP+ Technical Note for Validation of optical image matching tools, EDAP+.REP.029, in progress, 2023

RD-7. Bouvet, M.; Thome, K.; Berthelot, B.; Bialek, A.; Czapla-Myers, J.; Fox, N.P.; Goryl, P.; Henry, P.; Ma, L.; Marcq, S.; Meygret, A.; Wenny, B.N.; Woolliams, E.R. RadCalNet: A Radiometric Calibration Network for Earth Observing Imagers Operating in the Visible to Shortwave Infrared Spectral Range. Remote Sens. 2019, 11, 2401, https://doi.org/10.3390/rs11202401

RD-8. https://scihub.copernicus.eu/dhus/#/home Accessed online: 23 February 2023

RD-9.   Zanoni, "IKONOS Signal-to-Noise Ratio Estimation", March 25-27, 2002, JACIE Workshop, 2002 https://ntrs.nasa.gov/search.jsp?R=20040004380 Accessed online: 23 February 2023

RD-10. Françoise Viallefont-Robinet, Dennis Helder, Renaud Fraisse, Amy Newbury, Frans van den Bergh, Donghan Lee, Sébastien Saunier. Comparison of MTF measurements using edge method: towards reference data set. Optics Express, Optical Society of America, 2018, 26 (26), pp.33625-33648. ⟨hal-02055611⟩

RD-11. Blanc, P., Wald, L. 2009, A review of earth-viewing methods for in-flight assessment of modulation transfer function and noise of optical spaceborne sensors, https://www.researchgate.net/publication/259157057_A_review_of_earth-viewing_methods_for_in-flight_assessment_of_modulation_transfer_function_and_noise_of_optical_space-borne_sensors Accessed online: 23 February 2023

RD-12. J. Gil, MTF_Estimator, https://github.com/JorgeGIlG/MTF_Estimator Accessed online: 23 February 2023

RD-13. John Pike, National Image Interpretability Scale. 1998, https://fas.org/irp/imint/niirs.htm Accessed online: 23 February 2023

RD-14. F. Viallefont-Robinet et al. (2018), Comparison of MTF measurements using edge method: towards reference data set. Optics Express Vol. 26, No. 26, 33625, https://doi.org/10.1364/OE.26.033625

RD-15. EDAP Technical Note on Quality Assessment for SkySat, v1.0, EDAP.REP.015, 06/09/2021, https://earth.esa.int/eogateway/documents/20142/37627/Technical+Note+on+Quality+Assessment+for+SkySat.pdf/59a2a91d-eecd-20f1-4a13-e670dad8eed3

1.2   Acknowledgements

1.3   Glossary

The following acronyms and abbreviations have been used in this Report.

ACT	across-track
ALT	along-track
BRDF	Bidirectional Reflectance Distribution Function
EDAP	Earthnet Data Assessment Project
EO	Earth Observation
ESA	European Space Agency
ESF	Edge Spread Function , Edge Spread Function
FWHM	Full Width Half Maximum
GCP	ground control points
GIS	Geographic Information System

HR	High Resolution
JAXA	Japan Aerospace Exploration Agency
KLT	Kanade–Lucas–Tomasi
MTF	modulation transfer function
PICS	Pseudo-Invariant Calibration Sites
PSF	Point Spread Function , Point Spread Function
QA4EO	Quality Assurance Framework for Earth Observation
ROI	region of interest
SBAF	Spectral Band Adjustment Factor
SNR	signal-to-noise ratio
TOA	Top-of-Atmosphere
TPM	Third Party Mission
VHR	Very High Resolution

2.   EDAP+ ASSESSMENTS

2.1   Geometric Calibration Quality

The geometric calibration quality of product data is covered by the assessment of the absolute geolocation accuracy, temporal geolocation accuracy and band co-registration accuracy. The outputs of these three assessments ensure that the accuracy is described by the following metrics: the *mean offset* (systematic error contribution) and *standard deviation* (precision, random error contribution) in both directions (easting and northing), the *root mean square error* and the commonly reported *circular error* at the 90th percentile. The applicable metric(s) is then compared with the metric(s) used to describe the minimum performance requirement, stated by the mission provider, to determine if it is satisfied or not. It is important to note that the stated minimum performance requirement is commonly applicable to nadir-viewing acquisitions only.

Note for standard missions or standard products (e.g. orthorectified products), the optical team will only assess the horizontal (planimetric) and not the vertical geolocation accuracies.

2.1.1   Absolute Geolocation Accuracy Assessment

2.1.1.1   Methodology

The methodology adopted for this assessment, which is used to quantify the absolute displacement of objects or features of interest between the object space (i.e. true location) and image space (i.e. apparent location, following the geometric corrections implemented by the mission provider), depends on the spatial resolution of the product imagery being assessed. There are two methodologies that are used by the optical team and they are as follows:

a)   If the **spatial resolution** of the product imagery is $\lesssim$ **2.0 m** then the absolute accuracy is determined from the displacements measured between the true locations of a set of ground control points (**GCP**), defined by a global navigation satellite system (with a suitable positional accuracy) during a field survey, and their apparent locations in the product image. This is demonstrated in Figure 2-1.

Figure 2-1: (Left) The number and distribution of coverage of ground control points (+) from the field survey conducted in the area of La Crau, France. (Right) As an example, the apparent location of a ground control point (x) is located in the product image (e.g. panchromatic band) and the displacement is calculated by determining the difference between the true and apparent location.

b) If the **spatial resolution** of the product imagery is ⪆ **2.0 m** then the absolute accuracy is determined from the displacement measured by image matching product imagery (select an appropriate band, see Section 2.1.1.3), using a suitable image matching tool, with reference product imagery whose accuracy is known as high (acting as true location).

Note that as this data has a lower spatial resolution, the GCPs outlined in a) are on the limit of being resolved accurately by the human eye (therefore reducing pointing accuracy) and so data at this resolution are not really suitable for the GCP assessment.

2.1.1.2   Tools

The methodology described in a) in subsection 2.1.1.1 is conducted by the optical team using a shapefile of GCP and basic functionalities provided by QGIS [RD-4] (although, any Geographic Information System (**GIS**) software could be used).

The methodology described in b) in subsection 2.1.1.1 is conducted using the open-source, Python preliminary implementation of the KARIOS tool, based on the Kanade–Lucas–Tomasi (**KLT**) Feature Tracker, that has been validated, using SPOT reference data [RD-5] to produce sub-pixel accuracies [RD-6].

2.1.1.3   Reference Data

The main reference data selected for the methodology described in a) in subsection 2.1.1.1 are the two collections of ground control points, covering the regions of Salon-de-Provence (France, representing relatively flat and homogenous terrain) and Piedmont (Italy, representing relatively high and inhomogeneous terrain), that have been defined by the Differential Global Positioning System (0.25 m accuracy). The latter was acquired by field surveys conducted on behalf of ESA, for contribution to the Japan Aerospace Exploration Agency (**JAXA**) Advanced Land Observing Satellite's optical calibration / validation activities.

The reference data selected for the methodology described in b) in subsection 2.1.1.1 are selected from a suitable reference sensor, where the following factors are taken into consideration:

- The spatial coincidence should be maximised (i.e. footprint of the reference imagery should have a significant overlap with the footprint of the imagery produced by the sensor being assessed). The temporal and spectral coincidence should be maximised also, if possible. This was deemed necessary for the image matching tool used in the first phase of the project, which was based on an intensity-based algorithm, but the image matching tool to be used in this phase is based on a feature-based algorithm and so temporal and spectral coincidences are not as important.
- The spatial resolution of the imagery produced by the reference sensor should be as close as possible to the spatial resolution of the imagery produced by the sensor being assessed; image matching requires that the imagery being matched be of the same spatial resolution so the error introduced by resampling can be reduced. The imagery should also have the same projection.
- The geometric calibration quality of imagery produced by the reference sensor should be accurately quantified as high (these are often referred to as "gold standard" or baseline sensors).

2.1.2 Temporal Geolocation Accuracy Assessment

2.1.2.1 Methodology

The methodology adopted for this assessment is similar to that described for the assessment of the absolution geolocation accuracy, using the image matching tool, except that it requires that a sufficient number of product images covering a selected site and a sufficient period of time be assessed so that a suitable time series can be constructed (i.e. days since launch vs circular error). The timeseries is then subjected to linear regression (basic assumption), where the gradient x from the model $y = mx + c$ is used to quantify the temporal geolocation accuracy (i.e. geolocation stability).

2.1.2.2 Tools

This assessment is performed using the image matching tool described in Section 2.1.1.2.

2.1.2.3 Reference Data

This assessment does not make use of external reference data. The assessor should have the absolute geolocation accuracy of a selected band from a product image (i.e. panchromatic, red, or near-infrared band – larger spectral bandwidths translate to containing more 'information') quantified before using it as the reference image.

2.1.3 Band Co-registration Accuracy Assessment

2.1.3.1 Methodology

The method adopted for this assessment, which is commonly used to determine the geometric alignment of the bands (high quality alignment allows for the minimisation of geometric distortions and further processing such as band fusion), is based on image

matching adjacent band pairs in a given product image, e.g. multispectral band pairs (band 1,2), (band 2,3), (band 3,4).

In addition to the above, the error budget is computed (in this case, only for the multispectral bands), and it is based on the rule that per-pixel displacement errors are transitive across all band pairs — by summing the displacement for all band pairs, e.g. (1, 2), (2, 3), (3, 4), the result is in the same order of displacement, D, for the band pair (1, 4), as shown in the equation below:

$$D_{1,4} \cong D_{1,2} + D_{2,3} + D_{3,4}$$

Where $D_{1,4}$ stands for displacement between band 1 and 4 (calculated for the easting and northing direction).

By comparing this estimate $D_{1,4}$ against the true value ($D_{4,1}$) obtained with image matching, the error budget of the method is computed (i.e. error budget = $D_{1,4} + D_{4,1}$ or $D_{1,4} - D_{4,1}$).

2.1.3.2 Tools

This assessment is performed using the image matching tool described in Section 2.1.1.2.

2.1.3.3 Reference Data

This assessment does not make use of external reference data.

2.2 Radiometric Calibration Quality

The radiometric calibration quality of product imagery is covered by the assessment of the absolute and temporal radiometric accuracy.

The radiometric calibration, or correction, of sensor data sees to the successful conversion of raw data (i.e. digital numbers) to physical data such as spectral radiance or reflectance, using the provided calibration coefficients (e.g. physical bias, physical gain, solar spectral irradiance constants) that have been derived pre-flight / pre-launch (i.e. in laboratory conditions) or post-launch. This is important as it improves the interpretability and quality of the sensor data, and is particularly important when comparing multiple sensor datasets over a period of time, which is commonly performed by the scientific community.

2.2.1 Absolute Radiometric Accuracy Assessment

2.2.1.1 Methodology

The methodology adopted for this assessment, which is used to quantify the difference between the radiometric measurements detected at-sensor and true radiometric measurements (i.e. reference data from ground (i.e. *in situ*) or satellite-based sensors). The chosen methodology depends on the reference data selected and is described in the following sub-sections.

Note the reference data selected depends on the following factors:

- Reference data availability (e.g. continuous data is not available for all sites);

- Datetimes of acquisitions suitable for use with selected reference data;
- Spectral Band Adjustment Factor (**SBAF**) corrections (note SBAF corrections might not be needed if the spectral differences between the target and reference satellite sensor can be considered as negligible);
- Bidirectional Reflectance Distribution Function (**BRDF**), which is dependent on wavelength and describes the directional dependence of the reflected energy of a target as a function of solar and viewing geometries, and BRDF corrections (note BRDF corrections might not be needed if the solar and viewing geometries of the target and reference sensor are small, i.e. off-nadir angle < 5 °).

2.2.1.1.1   Methodology using RadCalNet Data

The RadCalNet calibration sites [RD-7], operated and maintained by the CEOS Working Group for Calibration and Validation of Infrared and Visible Optical Sensors, importantly provide the user community with the following:

- Top-of-Atmosphere (**TOA**) reflectances and their uncertainties, derived from both *in situ* surface and atmosphere measurements (e.g. surface pressure, columnar water vapour, columnar ozone, aerosol optical depth, etc.), that are SI-traceable, at:
    - 30-minute intervals between 09:00 and 15:00 local standard time (cloud-free data only), and 10-nm spectral sample intervals between 400 nm and 1000 nm.

It is important to note that this source of reference data is representative of nadir-viewing conditions only, and so any comparisons to sensor data with off-nadir viewing conditions should be used with caution and the relevant corrections taken into consideration. This is because when viewing zenith angle deviates significantly from nadir, both atmospheric and surface non-Lambertian behaviour can lead to significant deviations from nadir simulated signal.

To measure the absolute radiometric accuracy, the optical team will follow the methodology, for each measurement band, described in Figure 2-2.
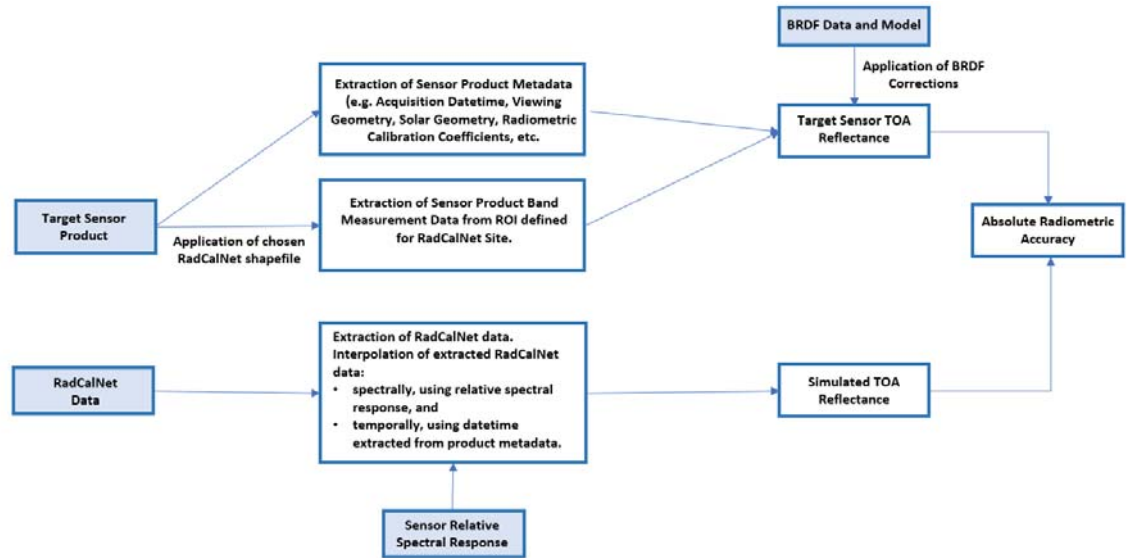
Figure 2-2: The methodology adopted when using RadCalNet data sourced from the RadCalNet portal (https://www.radcalnet.org/#!/).

The TOA reflectance measured by the target sensor, per band *b*, is estimated from the following steps:

1. The conversion from digital number to TOA radiance: the mean digital number (raw pixel value), extracted from the product band image using the applicable site shapefile (see example in Figure 2-3), is converted to the mean TOA radiance as follows:

$$L_b = DN_b * Gain_b + Bias_b$$

Where:

DN_b is the digital number (units: unitless)
$Gain_b$ is the physical gain (units: unitless)
$Bias_b$ is the physical bias (units: unitless)
L_b is the TOA radiance (units: $Wm^{-2}\mu m^{-1}$).

2. The conversion from TOA radiance to TOA reflectance: the mean TOA radiance (L_b) is converted to the mean TOA reflectance as follows:

$$\rho_b = \frac{\pi * L_b * d^2}{E_{0b} * Cos(\theta_s)}$$

Where:

E_{0b} is solar spectral irradiance at the sensor for band b (units: Wm^{-2})
θ_s is solar zenith angle at the time / location of acquisition (units: degrees)
d^2 is Sun–Earth distance at the time of acquisition (units: astronomical units)
ρ_b is TOA reflectance for band b (units: unitless).

It is important to note, depending on how the data provider wishes to provide its sensor data and accompanying information (e.g. coefficients, etc.), deviations to the above steps might be the case and so users should ensure that they follow the guidance provided by the data provider in the first instance.
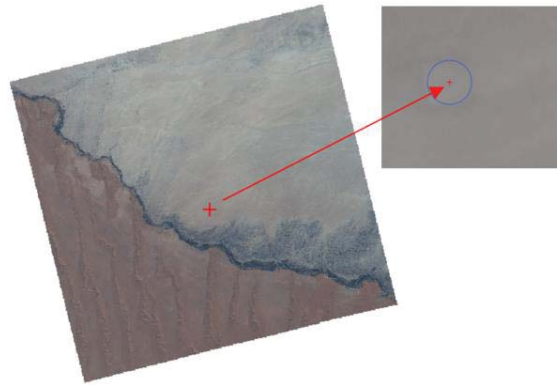
Figure 2-3: This RadCalNet site, one of five RadCalNet sites, is Gobabeb, Namibia. The shapefile is defined using the information provided for the site (latitude: -23.6002, longitude: 15.1196, altitude: 510 m. RadCalNet TOA reflectance spectra are representative of a disk of 30-m radius).

The absolute radiometric accuracy is then estimated by quantifying the difference, expressed as a percentage, between the target sensor TOA reflectance ($\rho_b\ work$) and simulated TOA reflectances ($\rho_b\ simulated$), from RadCalNet data, as follows:

$$\rho_b = ((\rho_b\ simulated - \rho_b\ work)/(\rho_b\ simulated)) * 100$$

2.2.1.1.2   Methodology using Satellite Data

This methodology would be adopted by the optical team if RadCalNet data is not available (the RadCalNet sites do not produce data for every day of the year).

The TOA reflectance measured by the target sensor is performed in the same way as described above, except that the region of interest (**ROI**) is defined over a more suitable site which should be as temporally, spatially and spectrally invariant as possible in order to distinguish more easily between potential changes (e.g. to a sensor's radiometric response and potential changes to the site surface and/or atmospheric characteristics). If applicable, BRDF corrections and/or SBAF corrections should be applied before estimating TOA reflectance.

The TOA reflectance measured by the reference sensor, using ideally a product image from a simultaneous or near simultaneous overpass (i.e. date and time of the two overpasses should be as close together as possible) of the defined ROI, is performed in the same way as described above. It is important to note that the data produced by the selected reference sensor should be very well radiometrically calibrated; baseline missions such as Landsat-8 OLI or Sentinel-2A/B MSI are considered appropriate [RD-8].

The absolute radiometric accuracy is then estimated by quantifying the difference, expressed as a percentage, between the target sensor TOA reflectance ($\rho_b\ work$) and reference sensor TOA reflectances ($\rho_b\ reference$) using the same formula as above except the comparison is reference rather than simulated.

2.2.1.2   Tools

The methodologies described above are implemented using Python code written in Jupyter notebooks.

2.2.1.3   Reference Data

The main forms of reference data used in the assessments performed by the optical team are mentioned in the subsection above. Although, there are many other sources of reference data that could be used for this assessment (e.g. Sentinel-2 MSI, Landsat 8). Additionally, the MODIS product mcd43a1v006 can be used for BRDF corrections.

2.2.2 Temporal Radiometric Accuracy Assessment

2.2.2.1   Methodology

The methodology adopted for this assessment, which provides an estimate of the radiometric stability, is based on measuring any changes to the TOA reflectance measured by target sensor of a suitable site over a sufficient period so that a suitable time series can be constructed (i.e. per band, days since launch vs estimated radiometric accuracy). The suitable site chosen is usually a site, such as one of the desert CEOS Pseudo-Invariant Calibration Sites (**PICS**) (https://calvalportal.ceos.org/pics_sites), that exhibits a high level of temporal, spatial and spectral invariance, enabled by minimising potential invariance to the site's surface (e.g. minimal signs of human settlement or other activities) and/or surrounding atmospheric conditions (e.g. minimal rainfall and cloud cover), so that potential changes to a sensor's radiometric response can be more easily distinguished.

The time series is then subjected to linear regression (basic assumption), where the gradient x from the model $y = mx + c$ is used to quantify the temporal radiometric accuracy (i.e. radiometric stability).

It is important to note that it is expected that data providers continuously perform their recalibration activities, as this is required to offset possible deviations as a result of sensor degradation.

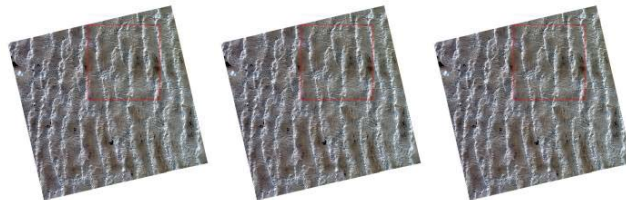Example outputs are shown in Figure 2-4 and Figure 2-5.

Figure 2-4: (Left) Target Acquisition 1 - Days Since Launch = 455, (Middle) Target Acquisition 2 - Days Since Launch = 503, (Right) Target Acquisition 3 - Days Since Launch = 527, over CEOS PICS Libya-4.
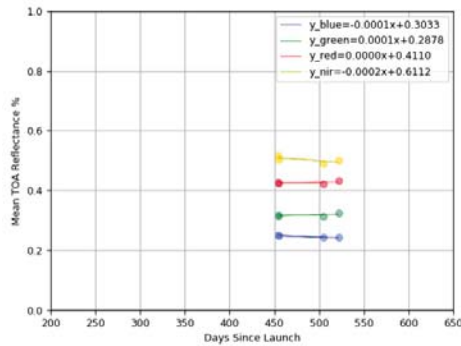
Figure 2-5: The radiometric stability of each spectral band (the mean TOA reflectance vs days since launch) for each product of the three products shown in Figure 2-4.

2.2.2.2   Tools

The methodology described above is implemented using Python code written in Jupyter notebooks by the optical team.

2.2.2.3   Reference Data

This assessment does not make use of external reference data.

2.3   Image Quality

The image quality is covered by the assessment of the signal-to-noise ratio, modulation transfer function and image interpretability.

2.3.1 Signal-to-Noise Ratio Assessment

2.3.1.1   Methodology

The signal-to-noise ratio (**SNR**) is used to determine the performance of a sensor in response to a particular exposure; it is based on quantifying the ratio of the sensor's output signal to the noise present in the output signal and can be expressed by the following:

$$SNR = \frac{\mu}{\sigma}$$

Where μ is the mean signal and σ is the standard deviation of the signal.

The method adopted for this assessment allows for the estimation of the spatial SNR, based on the aforementioned equation and the following assumption:

- The mean signal is defined as the spatial average of a group of pixels observing a spatially varying scene and the noise is defined as the standard deviation of this signal for the same group of pixels.

The method, which has been modified since it was initially proposed in [RD-9] in order to allow for the selection of small windows of uniform radiometric intensity (condition 1) and the selection of small windows mostly located over regions of flat terrain (condition 2), is

performed for each spectral band, whose imagery has been converted from digital numbers to TOA radiance, in the following way:

1. Compute the local statistics of a small, e.g. (9 x 9 pixels) sliding window applied to the imagery being assessed. Select only the "best" small windows for the following steps.
   a. The selection of small windows ensures that increased site uniformity is generally maintained. If it is not, where spatially high frequencies exist (e.g. sharp transitions seen as dune summits), dedicated image processing is applied in order to detect this and filter (e.g. using Sobel Filter).

2. Compute the statistical distribution (histogram), between the **minimum** and **maximum radiance**, of the selected "best" small windows – the signal is defined as the peak (i.e. mean radiance) of this statistical distribution and the noise is defined as the standard deviation of this statistical distribution about the mean.

3. Estimate SNR(s).
   a. The most accurate estimations of SNR are derived from statistical distributions that are of a normal (i.e. Gaussian) nature.

Note for this assessment, we use product imagery of a radiometrically bright PICS, defined by CEOS, such as Libya-4 (see https://calval.cr.usgs.gov/apps/libya-4).

2.3.1.2   Tools

This assessment is performed using an in-house python script that implements the methodology outlined above.

2.3.1.3   Reference Data

This assessment is not performed using external reference data.

2.3.2 Modulation Transfer Function Assessment

2.3.2.1   Methodology

The MTF, which is connected to the SNR (i.e. poor signal-to-noise ratio = poor sharpness) assessment, provides an estimate of image sharpness. There are a number of ways in which it can be measured but the most common, especially amongst the calibration/validation community, is the slanted-edge methodology [RD-10], [RD-11]. This methodology makes use of the following workflow:

1. Select a band from the product image and create a shapefile which defines the target edge to be used. Note the target edge must be straight and sharp (a man-made target is more likely to have these features), defined by a boundary between uniform high and low reflectance surfaces. Also, the target edge must be near vertical (i.e. the angle is important). This is an important requirement related to how the algorithm works — if an along-track or across-track assessment is needed then the image can be rotated accordingly (mathematically).
2. The data in each transect (each image row), defined by the shapefile, is smoothed and then differentiated in order to obtain a coarse estimation of the pixel position of the target edge. The latter estimation is then used to set the initial conditions of the

optimisation technique which is used to fit a sigmoid function to the data (as shown in Figure 2-6).
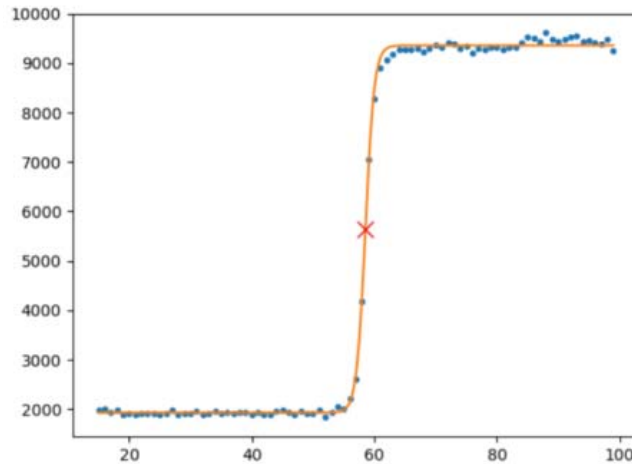

Figure 2-6: An example of the sigmoid function (–) fitted to the data (●) in one very sharp transect. The point of inflexion (X) shows the estimated sub-pixel edge position. X axis is pixels, y axis is digital numbers (figure from RD-12).

3. The estimated sub-pixel position for all transects is subjected to linear regression in order to ensure the target edge is straight as assumed (any outliers are removed during this process) and the target edge angle estimated.

4. The estimated sub-pixel edge position is used to shift each transect to a common origin, hence creating a supersampled virtual edge (green line in Figure 2-7) which is modelled (e.g. using a spline) and thus provides a representation of the Edge Spread Function (**ESF**), which is the red line in Figure 2-7.

5. The (two-dimensional) Point Spread Function (**PSF**) (blue line in Figure 2-7) is obtained by fitting the modelled shape to a one-dimensional Gaussian function (Line Spread Function) (brown line in Figure 2-7) using an optimisation function (e.g. Levenberg–Marquardt optimisation). Note the PSF defines the apparent shape of a point target as it appears in the resulting image: it is therefore directly related to the sharpness of images provided by the sensor/imaging system.
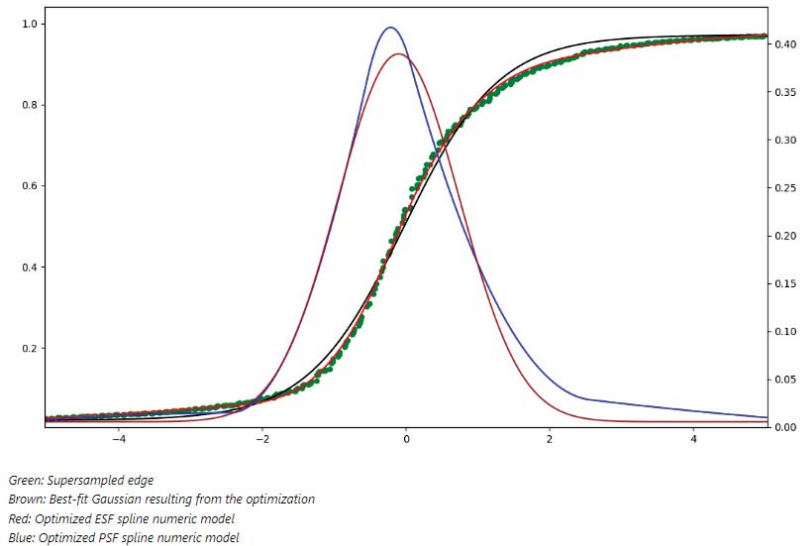
Green: Supersampled edge
Brown: Best-fit Gaussian resulting from the optimization
Red: Optimized ESF spline numeric model
Blue: Optimized PSF spline numeric model

Figure 2-7: Supersampled edge, ESF, Gaussian function and PSF example curves (figure from RD-12).

6. The MTF is then estimated from the modulus of the Fourier transform of the PSF. The MTF gives information on the contrast of the different spatial frequency components of the observed image.
7. The MTF at the Nyquist frequency is reported by the optical team in its assessment.

2.3.2.2 Tools

This assessment was performed in the first phase of the project using an in-house tool developed by Telespazio France. For the second phase of the project there will likely be the use of an additional tool, an open-source QGIS plugin, called the MTF Estimator [RD-12]. This tool is undergoing internal validation, in order to assure suitable performance [RD-6].

2.3.2.3 Reference Data

This assessment is not performed using external reference data.

2.3.3 Image Interpretability Assessment

2.3.3.1 Methodology

The image interpretability assessment provides a qualitative, rather than quantitative, assessment of image quality. The method adopted by the optical team is to identify and compare the interpretability of a set of points (features or objects) of interest in the product imagery from the sensor and in the product imagery from the reference sensor (again, using imagery from "gold standard" missions such as Pléiades). Note a more formal assessment can be derived using a set of points that have been recommended by National Imagery Interpretability Rating Scale [RD-13].

Note this assessment requires that the imagery from each sensor being compared is of the same spatial resolution (resampling could be appropriate) and it is most effective if the spectral qualities of the comparisons are the same, and they are from the same day and time to reduce shadow.

Figure 2-8: Image clips of a small collection of points of interest from the panchromatic band of a target sensor and reference sensor.

2.3.3.2 Tools

This assessment is performed using a simple script, written in Python, which performs the above activity, including generating the user-defined size clips of input band product imagery around the set of points (which are provided as input) and spatial resampling (using the Geospatial Data Abstraction Library `gdal_translate` utility).

2.3.3.3 Reference data

This assessment is performed using data from a sensor, selected as the reference sensor, that is known for producing very high-quality product imagery (e.g. Pléiades). In order to compare, the footprint of the data from the assessed sensor and the reference sensor should cover the geographic extent of most, if not all, points of interest listed.

2.4 Visual Inspections

2.4.1 Methodology

The methodology adopted for this assessment is relatively simple and only involves the visual inspection of the contents of the products (including product imagery (full-resolution, per band), metadata and auxiliary files, such as quality masks, etc.) in order to identify any anomalies or artefacts. Note this assessment is performed by the optical team first before the data is subjected to additional assessments.

2.4.2 Tools

The optical team commonly uses QGIS to visually inspect the contents of the products. However, the optical team and users can use other tools to browse the products should they wish (e.g. ESA SNAP Toolbox).

2.4.3 Reference Data

Reference data is not used for this assessment.

3. APPENDIX A: MTF TOOL ASSESSMENT

3.1 Introduction

The objective of this activity was to identify and validate a suitable, open-source MTF tool to support image quality assessments. Unfortunately, there was only one tool identified that was non-proprietary and freely available.

3.2 Candidate 1: MTF_Estimator QGIS Plugin

This open-source tool is used to robustly measure/estimate Edge Spread Function (**ESF**), Point Spread Function (**PSF**), Full Width Half Maximum (**FWHM**) and MTF from low-quality and synthetic images, using the slanted-edge methodology.

Author: Jorge Gil (Deimos Space)

Source Code: https://github.com/JorgeGIIG/MTF_Estimator

The source code is maintained and is very well documented (including a description of the algorithm). Demonstrations of its use, which is relatively straightforward, are provided. The tool (algorithm and implementation) has also been validated by the developer, using synthetic edges and actual edges, using third-party software.

3.3 Validation Assessment

The validation method used was to compare output (mean MTF @ Nyquist) generated by the tool with previous values from both the reference dataset used by the CEOS WGCV CalValPortal [RD-14] and output from the EDAP assessment of SkySat imagery (which used a different tool, but equivalent method) [RD-15].

3.3.1 CEOS WGCV Comparison

Full results have been provided to CEOS for assessment; a subset is shown below.

Error! Reference source not found. shows the Salon MTF target with the block layer used for MTF_Estimator analysis (left), and the graphical and statistical output from the tool (right). The key for the curves is:

Green: Supersampled edge

Brown: Best-fit Gaussian resulting from the optimization

Red: Optimized ESF spline numeric model

Blue: Optimized PSF spline numeric model

Image B: Salon MTF target

Angle: -10.217528
Smooth: 1.151132e-02
FWHM: 1.843706 px
MTF0: (0.9999999999999999+0j)
MTF30: 0.297437
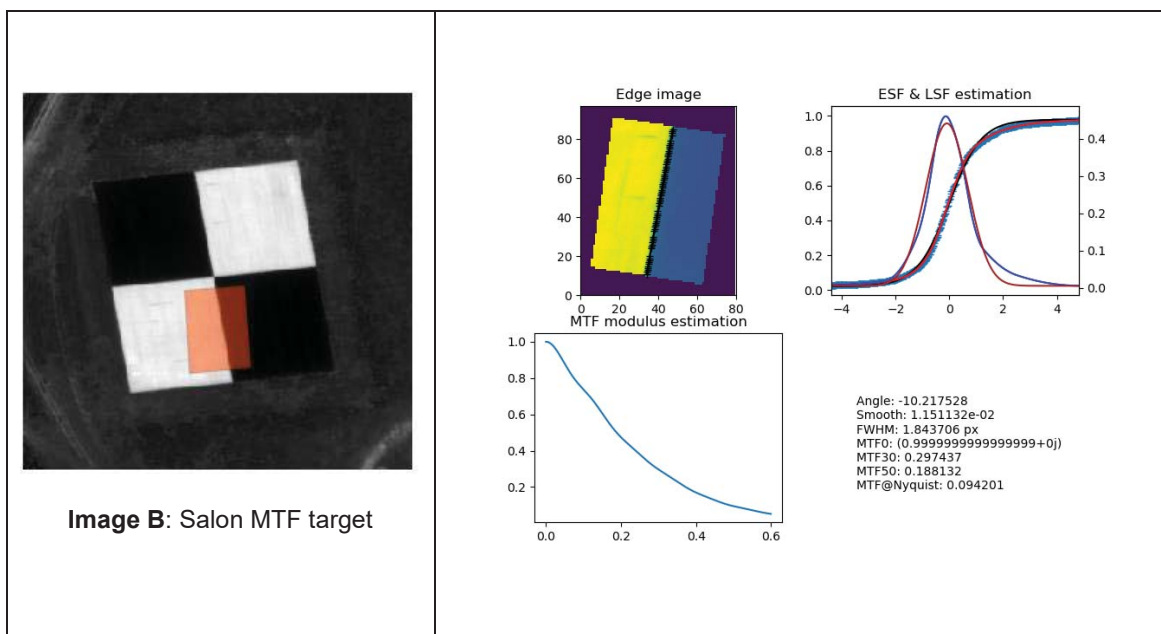MTF50: 0.188132
MTF@Nyquist: 0.094201

Figure 3-1: Salon MTF target with the block layer used for MTF_Estimator analysis (left), and the graphical and statistical output from the tool (right).

Table 3-1 shows the MTF@Nyquist frequency values (Mean, SD and Max-Min) for the CEOS reference images.

Table 3-1: MTF@Nyquist frequency values for the CEOS reference images. Images B and F are MTF targets (Salon and Big Spring, TX, respectively), images A, C, D and E are synthetic targets.

Image	Across track			Along-track		
	Mean	**SD**	**Max-Min**	**Mean**	**SD**	**Max-Min**
A	0.18	0.00	0.00	n/a	n/a	n/a
B	0.09	0.01	0.01	0.09	0.04	0.05
C	0.17	0.15	0.22	0.19	0.09	0.13
D	0.13	0.06	0.08	0.14	0.00	0.00
E	0.07	0.03	0.05	0.05	0.01	0.01
F	0.09	0.02	0.02	0.09	0.00	0.01

Image C has been identified as StdSystem_1, and Image E as StdSystem_30 from [RD-14. These are the only two we could identify unequivocally, and so below we present comparisons from the MTF_Estimator (MTFE) and the CEOS comparison exercise [RD-14] in the across-track (**ACT**) and along-track (**ALT**) directions.

Table 3-2: MTF at Nyquist Frequency: 1-m resolution (Image C and StdSystem_1)

	ACT		ALT	
	MTFE	**CEOS 2017b**	**MTFE**	**CEOS 2017b**
Mean	0.17	0.29	0.19	0.30
Std deviation	0.15	0.02	0.09	0.02
Max-min	0.22	0.04	0.13	0.04

Table 3-3: MTF at Nyquist Frequency: 30-cm resolution (Image E and StdSystem_30)

	ACT		ALT	
	MTFE	**CEOS 2017b**	**MTFE**	**CEOS 2017b**
Mean	0.07	0.10	0.05	0.09
Std deviation	0.03	0.01	0.01	0.01
Max-min	0.05	0.04	0.01	0.02

3.3.2 EDAP SkySat Analysis Comparison

The SkySat product that was used for MTF assessment within EDAP [RD-15], 20201229_112916_ssc17d2_0018_basic_analytic.tif, was also used for comparison. The original product was separated into R, G, B and NIR bands, the MTF_Estimator was applied and generated standard outputs.
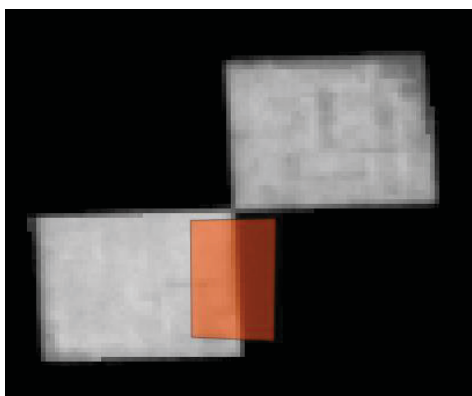

Figure 3-2: SkySat image used for MTF assessment (blue band shown).

To date, the SkySat image has been assessed in the ACT direction only, and the results are given in Table 3-4, which shows the comparison with the SkySat MTF assessment from the EDAP TN [RD-15]. The Vh and Vl directions are vertical edges with radiometries starting from high on the left to low on the right, and from low on the left to high on the right, respectively.

The average slant angle found for the SkySat image from the MTF_Estimator was -3.44 degrees.

Table 3-4: MTF comparison using SkySat image: comparison between the EDAP TN results [RD-15] and the MTF_Estimator (ACT directions only)

		EDAP TN		MTF_estimator	
		VH	VL	VH	VL
Blue	FWHM	2	2.5	2.24	1.93
	MTF@Nyquist	0.06	0.05	0.04	0.06
Green	FWHM	2.25	2.5	2.46	2.02
	MTF@Nyquist	0.045	0.035	0.03	0.04
Red	FWHM	2	2.25	-10.00	1.67
	MTF@Nyquist	0.035	0.031	0.07	0.07
NIR	FWHM	2.5	2.25	2.96	1.77
	MTF@Nyquist	0.02	0.04	0.01	0.05

Table 3-4 shows a good correspondence between the EDAP SkySat TN [RD-15] and the MTF_Estimator, except for the Red band; the MTF_Estimator was unable to generate a PSF from the image, as evidenced by the anomalous -10 pixel measurements for FWHM.

3.4   Summary

Although independent confirmation from CEOS has not been forthcoming at the time of issue of this report, the comparison with SkySat imagery assessment that took place within EDAP has provided a measure of external verification of the MTF_Estimator. Apart from the trouble that the MTFE had with the red band image (and this could likely be revisited by arranging a different analysis box) the comparisons for FWHM and MTF@Nyquist frequency are of comparable order that we have confidence in the use of the MTF_Estimator for EDAP+ Optical assessments.

[END OF DOCUMENT]